ISSN 0021-3640, JETP Letters, 2006, Vol. 84, No. 12, pp. 650–655. © Pleiades Publishing, Inc., 2006.

Electronic Theory for Itinerant In-Plane Magnetic Fluctuations in Na_xCoO_2¶

M. M. Korshunov[a, b], I. Eremin[b, c], A. Shorikov[d], and V. I. Anisimov[d]

[a] *Kirensky Institute of Physics, Siberian Division, Russian Academy of Sciences, Krasnoyarsk, 660036 Russia*

[b] *Max-Planck-Institut für Physik komplexer Systems, D-01187 Dresden, Germany*

e-mail: maxim@mpipks-dresden.mpg.de

[c] *Institut für Mathematische Physik and Theoretische Physik, TU Braunschweig, 38106 Braunschweig, Germany*

[d] *Institute of Metal Physics, Ural Division, Russian Academy of Sciences, Yekaterinburg GSP-170, 620041 Russia*

Received October 30, 2006

Starting from the ab initio band structure for Na_xCoO_2, we derive the single-electron energies and the effective tight-binding description for the t_{2g} bands using a projection procedure. We find that, due to the presence of the next-nearest-neighbor hoppings, a local minimum in the electronic dispersion close to the Γ point of the first Brillouin zone forms. Therefore, in addition to a large Fermi surface, an electron pocket close to the Γ point emerges at high doping concentrations. The latter yields a new scattering channel resulting in the peak structure of the itinerant magnetic susceptibility at low momenta. This indicates an itinerant in-plane ferromagnetic state above a certain critical concentration x_m, which is in agreement with neutron scattering data. Below x_m, the magnetic susceptibility shows a tendency towards antiferromagnetic fluctuations. We estimate the value of $0.56 < x_m < 0.68$ within the rigid band model and within the Hubbard model with infinite on-site Coulomb repulsion consistent with the experimental phase diagram.

PACS numbers: 31.15.Ar, 71.10.-w, 74.70.-b, 75.40.Cx

DOI: 10.1134/S0021364006240040

1. The diverse physical properties of the cobaltate Na_xCoO_2 attracted much attention after the discovery of the unconventional superconductivity in its hydrated counterpart, $Na_xCoO_2 \cdot yH_2O$ [1]. The phase diagram of this compound, with varying electron doping x and water intercalation y, is rich and complicated; in addition to superconductivity, it exhibits magnetic and charge orders and some other structural transitions [2–5]. The parent compound, Na_xCoO_2, is a quasi-two-dimensional system with Co in CoO_2 layers forming a triangular lattice where the Co–Co in-plane distance is three times smaller than the interplane one. An Na ion resides between the CoO_2 layers and gives additional x electrons to the layer, thus, lowering the Co valence from Co^{4+} ($3d^5$ configuration) to Co^{3+} ($3d^6$ configuration) upon x changing from 0 for the virtual compound CoO_2 to 1 for $NaCoO_2$. The hole in the d orbital occupies one of the t_{2g} levels, which are lower than the e_g levels by about 2 eV [6]. The degeneracy of the t_{2g} levels is partially lifted by the trigonal distortion, which splits it into the higher a_{1g} singlet and the lower two e_g' states.

The first principle LDA (local density approximation) and LDA + U band structure calculations predict Na_xCoO_2 to have a large Fermi surface (FS) with mainly a_{1g} character and centered around the $\Gamma = (0, 0, 0)$ point and also six hole pockets of mostly e_g' character near the $K = (0, 4\pi/3, 0)$ points of the hexagonal Brillouin zone for a wide range of x [6, 7]. At the same time, recent Angle-Resolved Photo-Emission Spectroscopy (ARPES) experiments [8–11] reveal doping dependent Fermi surface evolution for a wide range of Na concentrations ($0.3 \le x \le 0.8$) with no sign of the hole pockets. The observed Fermi surface is centered around the Γ point and has a mostly a_{1g} character. Furthermore, the measured dispersion of the top of the valence band is twice as narrower as compared to the LDA calculated bands.

Concerning the magnetic properties, the local spin density approach (LSDA) predicts Na_xCoO_2 to have a weak intraplane itinerant ferromagnetic (FM) state for almost all Na concentrations $0.3 \le x \le 0.7$ [12]. On the contrary, neutron scattering finds the A-type antiferromagnetic order implying the ferromagnetic order within the Co layer only for $0.75 \le x \le 0.9$ with an ordering temperature of $T_m \approx 22$ K with the interplane J_c and intraplane J_{ab} exchange constants being 12 meV and –6 meV, respectively [13–15].

In this letter, we derive an effective low-energy model describing the bands crossing the Fermi level on the basis of the LDA band structure calculations. Due to the FS topology, which is inferred from the LDA

¶ The text was submitted by the authors in English.

band structure, the magnetic susceptibility $\chi_0(\mathbf{q}, \omega = 0)$ reveals two different regimes for different dopings: for $x < 0.58$, it shows pronounced peaks at the antiferromagnetic (AFM) wave vector $\mathbf{Q}_{\mathrm{AFM}} = \{(2\pi/3, 2\pi/\sqrt{3}), (4\pi/3, 0)\}$ resulting in the tendency towards the in-plane 120° AFM order, while, for $x > 0.58$, the peaks at low momenta near the $\mathbf{Q}_{\mathrm{FM}} = (0, 0)$ form clearly demonstrating the tendency of the system towards the itinerant in-plane FM ordered state. We find that the formation of the electron pocket around the Γ point is crucial for the in-plane FM ordering at high doping concentrations.

2. The band structure of $Na_{0.33}CoO_2$ (Fig. 1) was obtained within the LDA [16] in the framework of the TB-LMTO-ASA (tight binding approach to the LMTO using atomic sphere approximation) [17] computation scheme. The crystal structure parameters were taken from [18]. The bands crossing the Fermi level have mostly an a_{1g} character, which is consistent with previous LDA findings [6]. Note that the small FS pockets near the K point with e'_g-symmetry present at $x = 0.33$ disappear for higher dopings because the corresponding bands sink below the Fermi level.

To construct the effective Hamiltonian and to derive the effective Co–Co hopping integrals $t_{fg}^{\alpha\beta}$ for the t_{2g}-manifold, we apply the projection procedure [19, 20]. Here, $(\alpha\beta)$ denotes a pair of orbitals: a_{1g}, e'_{g1} or e'_{g2}. The indices f and g correspond to the Co sites on the triangular lattice. The obtained hoppings are given in the table, and the obtained single-electron energies ε^{α} are equal to the following (in eV, relative to $\varepsilon^{a_{1g}}$): $\varepsilon^{a_{1g}} = 0$, $\varepsilon^{e'_{g1}} = \varepsilon^{e'_{g2}} = -0.053$.

A comparison between the bands obtained using the projection procedure and the LDA bands is shown in Fig. 1, which confirms the Co–t_{2g} nature of the near-Fermi level bands [6, 21]. For simplicity, we have enumerated the site pairs $t_{fg}^{\alpha\beta} \longrightarrow t_n^{\alpha\beta}$ with $n = 0, 1, 2, \ldots$ (see Fig. 2a and the correspondence between the in-plane vectors and the index n in the table). Due to the C_3 symmetry of the cobaltate lattice, the following equalities are present: $|t_3^{\alpha\beta}| = |t_1^{\alpha\beta}|$, $|t_5^{\alpha\beta}| = |t_4^{\alpha\beta}|$, and $|t_9^{\alpha\beta}| = |t_7^{\alpha\beta}|$. In addition, $t_1^{\alpha\beta} = t_2^{\alpha\beta}$ for $a_{1g} \longrightarrow a_{1g}$ hoppings, which, however, does not hold for $e'_{g1,2}$ orbitals. Thus, since the hybridization between the a_{1g} and the e'_g bands is not small, a simplified description of the bands crossing the Fermi level in terms of the a_{1g} band

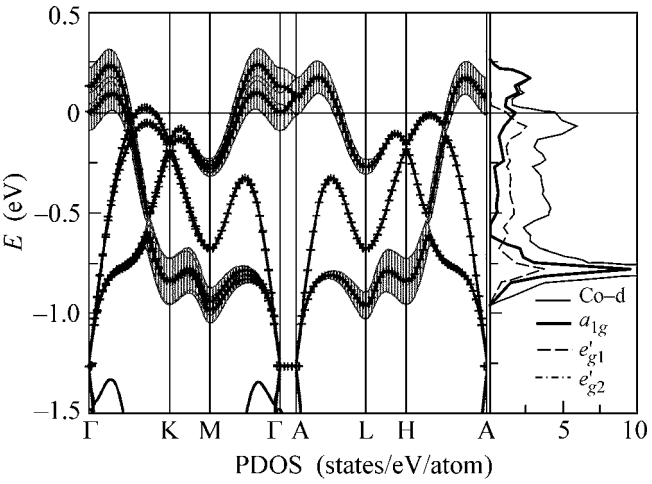

Fig. 1. Calculated near-Fermi level LDA band structure and partial density of states (PDOS) for $Na_{0.33}CoO_2$. The contribution of Co-a_{1g} states is denoted by the vertical broadening of the bands with thickness proportional to the weight of the contribution. The crosses indicate the dispersion of the bands obtained by projection on the t_{2g} orbitals.

In-plane hopping integrals $t_n^{\alpha\beta}$ for different in-plane vectors $n = (f, g)$ for Na_xCoO_2, $x = 0.33$

$n = (f, g)$	(0, 1)	$\left(\frac{\sqrt{3}}{2}, \frac{1}{2}\right)$	$\left(\frac{\sqrt{3}}{2}, -\frac{1}{2}\right)$	$(\sqrt{3}, 0)$	$\left(\frac{\sqrt{3}}{2}, \frac{3}{2}\right)$	$\left(\frac{\sqrt{3}}{2}, -\frac{3}{2}\right)$	(0, 2)	$(\sqrt{3}, 1)$	$(\sqrt{3}, -1)$
$\alpha \longrightarrow \beta$	$t_1^{\alpha\beta}$	$t_2^{\alpha\beta}$	$t_3^{\alpha\beta}$	$t_4^{\alpha\beta}$	$t_5^{\alpha\beta}$	$t_6^{\alpha\beta}$	$t_7^{\alpha\beta}$	$t_8^{\alpha\beta}$	$t_9^{\alpha\beta}$
$a_{1g} \longrightarrow a_{1g}$	0.123	0.123	0.123	−0.022	−0.022	−0.021	−0.025	−0.025	−0.025
$a_{1g} \longrightarrow e'_{g1}$	−0.044	0.089	−0.044	0.010	0.010	−0.021	−0.021	0.042	−0.021
$a_{1g} \longrightarrow e'_{g2}$	−0.077	0.000	0.077	0.018	−0.018	0.000	−0.036	0.000	0.036
$e'_{g1} \longrightarrow e'_{g1}$	−0.069	−0.005	−0.069	0.018	0.018	−0.026	−0.017	−0.085	−0.017
$e'_{g1} \longrightarrow e'_{g2}$	0.037	0.000	−0.037	−0.026	0.026	0.000	−0.039	0.000	0.039
$e'_{g2} \longrightarrow e'_{g2}$	−0.026	−0.090	−0.027	−0.011	−0.011	0.033	−0.062	0.006	−0.062

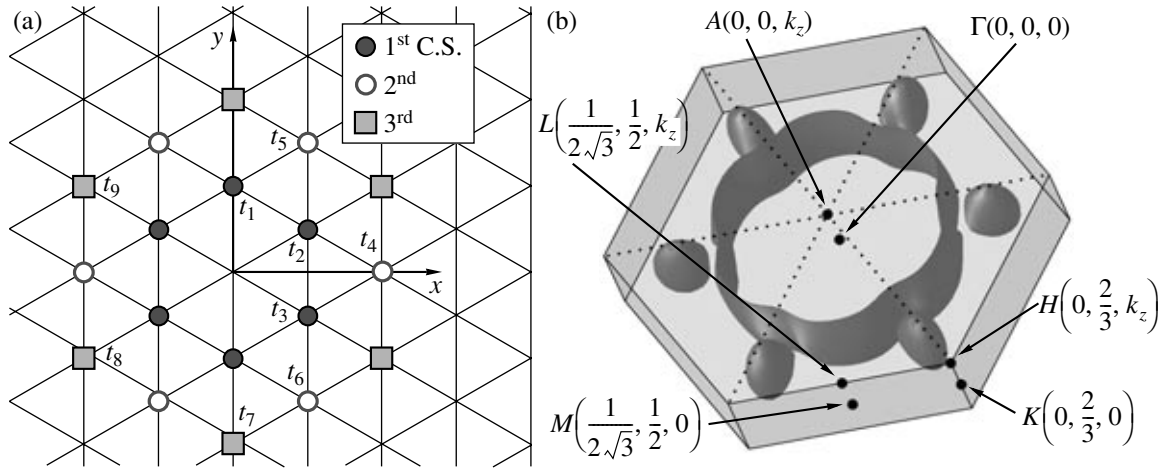

Fig. 2. (a) Schematic crystal structure of the Co layer in Na_xCoO_2 with hopping notations within the first three coordination spheres (C.S.). (b) LDA-calculated Fermi surface with the cylindrical part having mostly a_{1g} character and six hole pockets having mostly e'_g character. The k_x and k_y coordinates of the symmetry points are given in units of $2\pi/a$ with a being the in-plane lattice constant.

only (neglecting the e'_g band and the corresponding hybridizations; see, e.g., [22]) may lead to an incorrect result due to its higher symmetry. In the following, we neglect the interlayer splitting present for the $k_z = 0$ plane because of its subtle effect on the topology of the FS [6].

Then, the free electron Hamiltonian for the CoO_2-plane in a hole representation is given by

$$H_0 = -\sum_{\mathbf{k},\alpha,\sigma}(\varepsilon^{\alpha}-\mu)n_{\mathbf{k}\alpha\sigma} - \sum_{\mathbf{k},\sigma}\sum_{\alpha,\beta} t_{\mathbf{k}}^{\alpha\beta} d^{\dagger}_{\mathbf{k}\alpha\sigma} d_{\mathbf{k}\beta\sigma}, \quad (1)$$

where $d_{\mathbf{k}\alpha\sigma}$ ($d^{\dagger}_{\mathbf{k}\alpha\sigma}$) is the annihilation (creation) operator for the hole with the momentum $\mathbf{k}$, spin σ, and orbital index α, $n_{\mathbf{k}\alpha\sigma} = d^{\dagger}_{\mathbf{k}\alpha\sigma} d_{\mathbf{k}\alpha\sigma}$; and $t_{\mathbf{k}}^{\alpha\beta}$ is the Fourier transform of the hopping matrix element. Introducing the matrix notations $(\hat{t}_{\mathbf{k}})_{\alpha\beta} = t_{\mathbf{k}}^{\alpha\beta}$ and $(\hat{t}_n)_{\alpha\beta} = t_n^{\alpha\beta}$, the hoppings matrix elements in the momentum representation are given by

$$\begin{aligned}\hat{t}_{\mathbf{k}} &= 2\hat{t}_1\cos k_2 \\ &+ 2\hat{t}_2\cos k_3 + 2\hat{t}_3\cos k_1 + 2\hat{t}_4\cos(k_1+k_3) \\ &+ 2\hat{t}_5\cos(k_2+k_1) + 2\hat{t}_6\cos(k_1-k_2) \\ &+ 2\hat{t}_7\cos 2k_2 + 2\hat{t}_8\cos 2k_3 + 2\hat{t}_9\cos 2k_1,\end{aligned} \quad (2)$$

where $k_1 = \frac{\sqrt{3}}{2}k_x - \frac{1}{2}k_y$, $k_2 = k_y$, $k_3 = \frac{\sqrt{3}}{2}k_x + \frac{1}{2}k_y$.

Within this rigid band approximation, the doping-dependent evolution of the electronic dispersion, the density of states (DOS), and the FS is shown in Fig. 3. We notice that, already at $x = 0.48$, the FS e'_g hole pockets are absent. Most importantly, we find another interesting feature. Namely, the local minimum of the band dispersion around the Γ point yields the appearance of the second FS contour centered around this point. This electron FS pocket becomes larger upon increasing doping x. As was shown in [23] for the Hubbard model on a triangular lattice, the main reason for the local minimum around the Γ point is the presence of the next-nearest-neighbor hoppings, which also enter in our calculations.

Although this minimum is not yet directly observed in ARPES experiments, the presence of the associated second FS contour would reduce the FS volume and resolve the issue why the volume of the FS observed in ARPES is larger than is expected from Luttinger theorem [24]. Furthermore, an emergence of this pocket would influence the Hall conductivity at high doping concentrations, which is interesting to check experimentally.

3. To analyze the possibility of itinerant magnetism, we calculate the magnetic susceptibility $\chi_0(\mathbf{q}, \omega = 0)$ based on the Hamiltonian H_0. The doping-dependent evolution of the peaks in $\mathrm{Re}\chi_0(\mathbf{q}, 0)$ is shown in Fig. 4. At $x = 0.45$, the e'_g bands are below the Fermi level and the FS has the form of a rounded hexagon. This results in a number of nesting wave vectors around the antiferromagnetic wave vector $\mathbf{Q}_{\mathrm{AFM}}$. The corresponding broad peaks in the $\mathrm{Re}\chi_0(\mathbf{q}, 0)$ appear around $\mathbf{Q}_{\mathrm{AFM}}$, indicating the tendency of the electronic system towards the 120° AFM ordered state [25]. Upon increasing doping, the Fermi level crosses the local minimum at the Γ point, resulting in the second almost circle FS contour. As soon as this change of the FS topology takes place, the scattering at the momentum $\mathbf{Q}_{\mathrm{AFM}}$ is quickly suppressed, and it vanishes already at

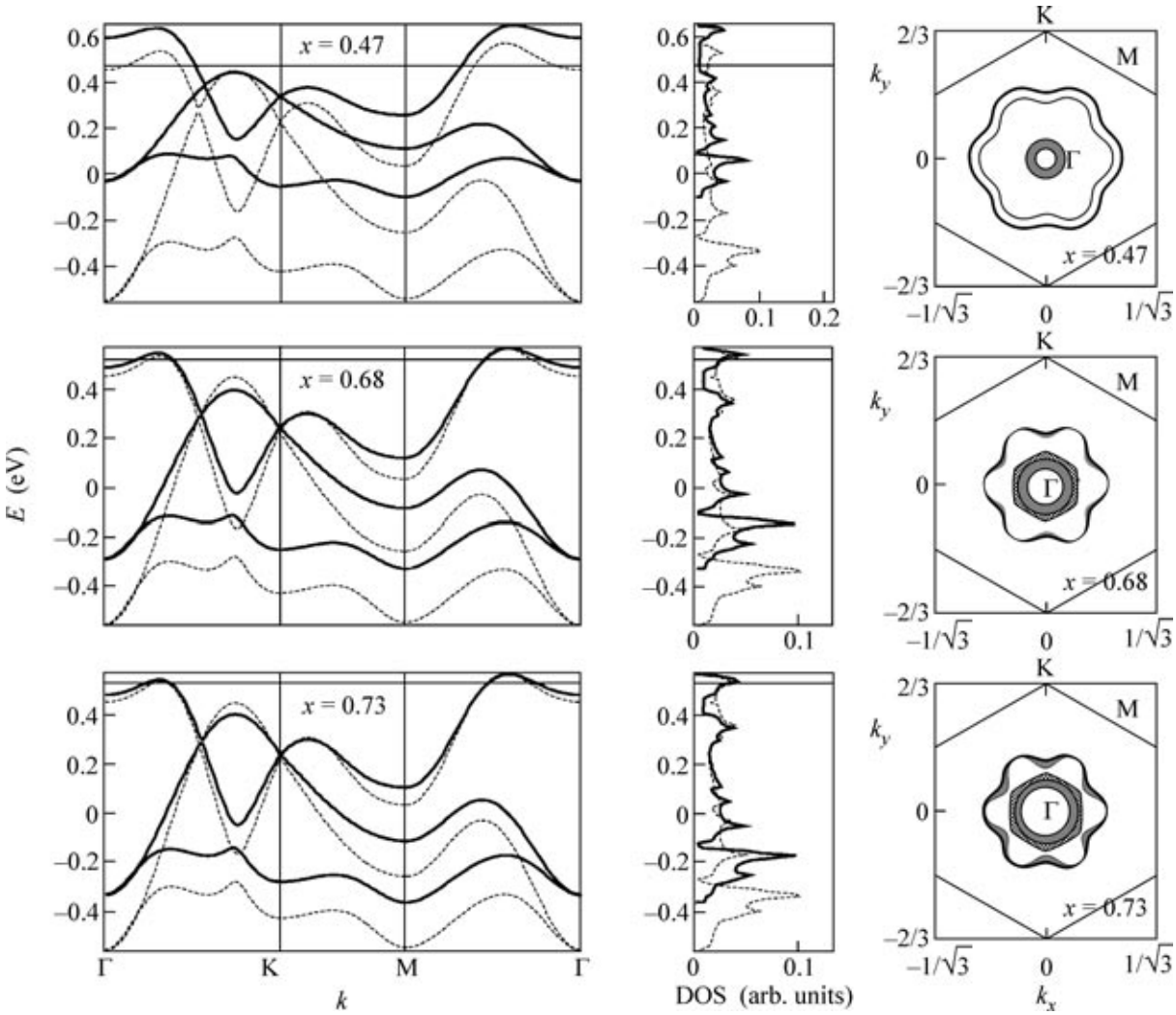

Fig. 3. Calculated band structure and Fermi surface for Na_xCoO_2 for $x = 0.47$, 0.68, and 0.73. The dashed (light gray) and solid (black) curves represent the rigid-band approximation and the Hubbard-I solution, respectively. The horizontal line denotes the self-consistently calculated chemical potential μ.

$x_m \approx 0.56$. Most importantly, a new scattering vector, $\mathbf{Q}_1$, appears. This wave vector is small and yields peaks in the magnetic susceptibility at low momenta, indicating the tendency of the magnetic system to shift towards itinerant FM order. For larger x, the inner FS contour increases leading to a further decrease of the $\mathbf{Q}_1$. In the case of $x \approx 0.88$, the FS topology changes again, resulting in a six distant FS contours yielding an even smaller length of $\mathbf{Q}_1$. The obtained scattering at low momenta in the magnetic susceptibility for $x > x_m$ is qualitatively consistent with the scattering around $\mathbf{Q}_{FM} = (0, 0)$ observed in the neutron scattering experiments [13–15].

4. Since the obtained magnetic susceptibility depends mostly on the topology of the FS, one expects that the behavior shown in Fig. 4 will be valid even if one takes the interaction term H_{int} into account, at least in the case if it is the on-site Hubbard interaction U. The only difference would be a shift of the critical concentrations x_m, at which the FS topology changes and the tendency to the AFM order changes towards the FM ordered state. To check this, we have taken the strong electron correlations into account by adding the on-site Coulomb interaction terms to H_0 similar to [26, 27]. The effective on-site Hubbard repulsion $U_{eff} \approx 4$ eV on the Co sites is much larger than the bare bandwidth $W \approx 1.2$ eV, and, thus, it is possible to project doubly occupied states out and formulate an effective model equivalent to the Hubbard model with an infinite value of U.

In the atomic limit, local low-energy states on the Co sites are the vacuum state $|0\rangle$ and the single-hole states $|a\sigma\rangle$, $|e_1\sigma\rangle$, $|e_2\sigma\rangle$. The simplest way to describe the quasiparticle excitations between these states is to use the projective Hubbard X-operators [28]: $X_f^m \longleftrightarrow$

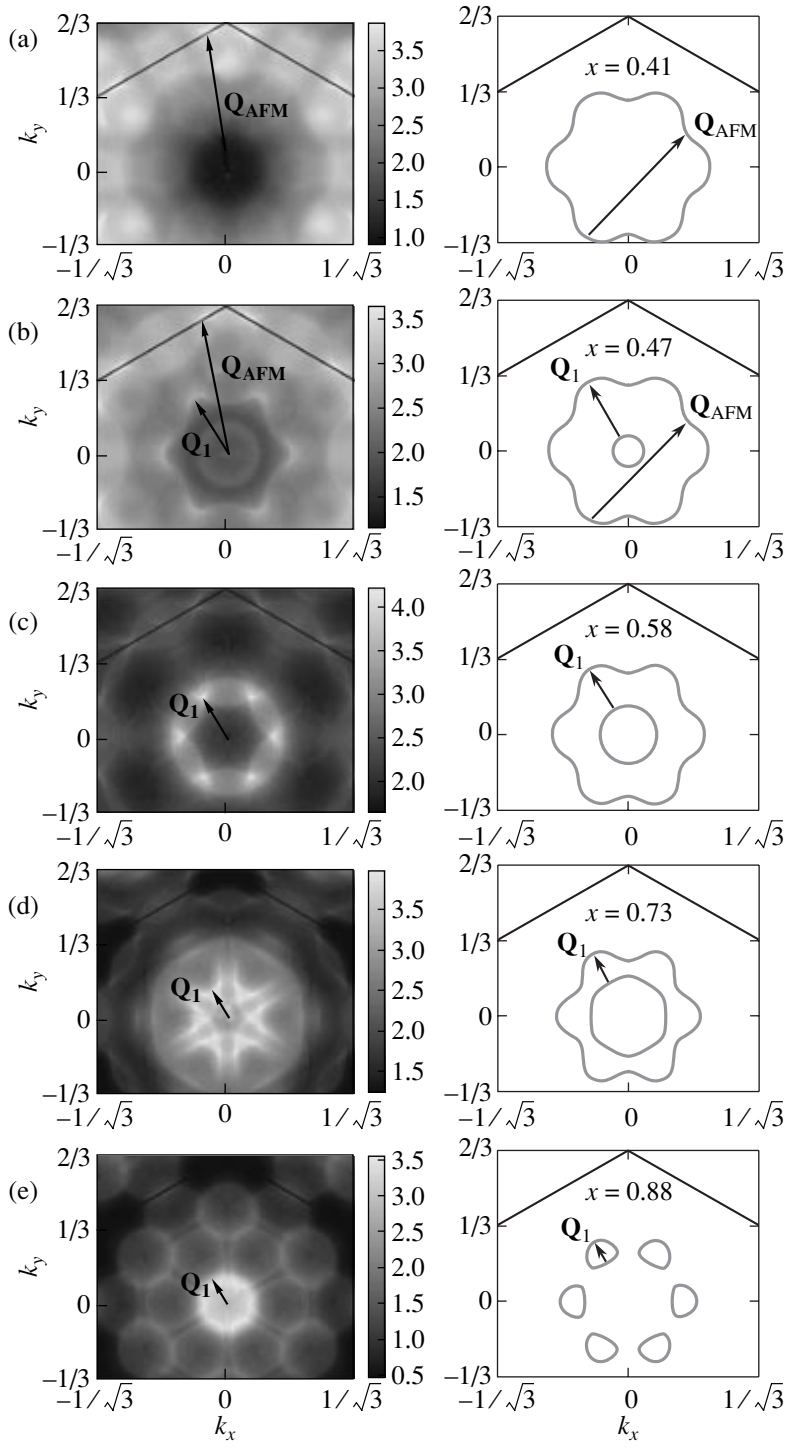

Fig. 4. Grayscale plot of the real part of the magnetic susceptibility $\mathrm{Re}\chi_0(\mathbf{k}, \omega = 0)$ as a function of the momentum in units of $2\pi/a$ (left), and the Fermi surface for the corresponding doping x (right). The arrows indicate the scattering wave vectors $\mathbf{Q_i}$ as described in the text.

$X_f^{p,q} \equiv |p\rangle\langle q|$, where the index $m \longleftrightarrow (p, q)$ enumerates quasiparticles. There is a simple correspondence between the X-operators and single-electron creation–annihilation operators: $d_{f\alpha\sigma} = \sum_m \gamma_{\alpha\sigma}(m) X_f^m$, where $\gamma_{\alpha\sigma}(m)$ determines the partial weight of a quasiparticle m with spin σ and orbital index α. In these notations,

the Hamiltonian of the Hubbard model in the limit $U \longrightarrow \infty$ has the form

$$H = -\sum_{f,p}(\varepsilon^p - \mu)X_f^{p,p} - \sum_{f \neq g}\sum_{m,m'} t_{fg}^{mm'} X_f^{m\dagger} X_g^{m'}. \quad (3)$$

In the so-called Hubbard-I approximation within the generalized Dyson equation for the X-operators [29–31], the quasiparticle bands formed by the $a_{1g} \longrightarrow a_{1g}$ hoppings will be renormalized by the $(1 + x)/2$ factor, while the quasiparticle bands formed by the e_g' hoppings will be renormalized by x.

In Fig. 3, the quasiparticle spectrum is shown. One finds that, within the Hubbard-I approximations, the bands become narrower with lowering x due to the doping dependence of the quasiparticle spectral weight. Most importantly, the doping evolution of the FS is qualitatively the same as in the rigid-band picture. Thus, the bandwidth reduction and spectral weight renormalization do not change the topology of the FS. Therefore, the presence of the strong electronic correlations does not qualitatively change our results for the bare susceptibility. Quantitatively, the critical concentration x_m shifts towards higher values, and within Hubbard-I it becomes $x_m \approx 0.68$.

5. To conclude, we have shown that, in the model with *ab-initio* calculated parameters, the magnetic susceptibility is doping dependent. At the critical doping concentration, x_m, the electron pocket on the FS in the center of the Brillouin zone well develops. For $x < x_m$, the system shows a tendency towards the 120° AFM ordered state, while, for $x > x_m$, the peak in the magnetic susceptibility is at small wave vectors, thus, indicating a strong tendency towards the itinerant FS state. Within the tight-binding model, x_m is estimated to be around 0.56. Analyzing the influence of the strong Coulomb repulsion and the corresponding reduction of the bandwidth and the quasiparticle spectral weight in the strong-coupling Hubbard-I approximation, we show that the critical concentration changes to $x_m \approx 0.68$. At the same time, the underlying physics of the formation of the itinerant FM state remains the same.

We are grateful to G. Bouzerar, W. Brenig, P. Fulde, S.G. Ovchinnikov, D. Singh, and Z. Wang for useful discussions; to I. Mazin and N.B. Perkins for the careful reading of the manuscript; and S. Borisenko for sharing with us the experimental results prior to publication. The work of M.M.K. was supported by INTAS YS (grant no. 05-109-4891) and the Russian Foundation for Basic Research (project nos. 06-02-16100 and 06-02-90537-BNTS). A.S. and V.I.A. acknowledge the support of the Russian Foundation for Basic Research (project nos. 04-02-16096 and 06-02-81017) and the NWO (grant no. 047.016.005).

REFERENCES

1. K. Takada et al., Nature **422**, 53 (2003).
2. I. Terasaki, Y. Sasago, and K. Uchinokura, Phys. Rev. B **56**, 12 685(R) (1997).
3. Y. Wang et al., Nature **423**, 425 (2003).
4. M. L. Foo et al., Phys. Rev. Lett. **92**, 247001 (2004).
5. B. C. Sales et al., Phys. Rev. B **70**, 174419 (2004).
6. D. J. Singh, Phys. Rev. B **61**, 13397 (2000).
7. K.-W. Lee, J. Kuneš, and W. E. Pickett, Phys. Rev. B **70**, 045104 (2004).
8. M. Z. Hasan et al., Phys. Rev. Lett. **92**, 246402 (2004).
9. H.-B. Yang et al., Phys. Rev. Lett. **92**, 246403 (2004).
10. H.-B. Yang et al., Phys. Rev. Lett. **95**, 146401 (2005).
11. D. Qian et al., Phys. Rev. Lett. **96**, 216405 (2006).
12. D. J. Singh, Phys. Rev. B **68**, 020503(R) (2003).
13. A. T. Boothroyd et al., Phys. Rev. Lett. **92**, 197201 (2004).
14. S. P. Bayrakci et al., Phys. Rev. Lett. **94**, 157205 (2005).
15. L. M. Helme et al., Phys. Rev. Lett. **94**, 157206 (2005).
16. W. Kohn and L. J. Sham, Phys. Rev. A **140**, 1133 (1965).
17. O. K. Andersen and O. Jepsen, Phys. Rev. Lett. **53**, 2571 (1984).
18. J. D. Jorgensen et al., Phys. Rev. B **68**, 214517 (2003).
19. N. Marzari and D. Vanderbilt, Phys. Rev. B **56**, 12 847 (1997).
20. V. I. Anisimov et al., Phys. Rev. B **71**, 125119 (2005).
21. M. D. Johannes et al., Europhys. Lett. **68**, 433 (2004).
22. K. Kuroki et al., Phys. Rev. B **73**, 184503 (2006).
23. M. Renner and W. Brenig, cond-mat/0310244 (unpublished).
24. S. Borisenko, private communication.
25. M. D. Johannes et al., Phys. Rev. Lett. **93**, 097005 (2004).
26. S. Zhou et al., Phys. Rev. Lett. **94**, 206401 (2005).
27. M. Indergand et al., Phys. Rev. B **71**, 214414 (2005).
28. J. C. Hubbard, Proc. R. Soc. London, Ser. A **277**, 237 (1964).
29. R. O. Zaitsev, Sov. Phys. JETP **41**, 100 (1975).
30. Yu. Izumov and B. M. Letfullov, J. Phys.: Condens. Matter **3**, 5373 (1991).
31. S. G. Ovchinnikov and V. V. Val'kov, *Hubbard Operators in the Theory of Strongly Correlated Electrons* (Imperial College Press, London, 2004).